Journal of Power Sources 267 (2014) 881–887

Contents lists available at ScienceDirect

Journal of Power Sources

journal homepage: www.elsevier.com/locate/jpowsour

Fabrication of all-solid-state battery using epitaxial $LiCoO_2$ thin films

Susumu Shiraki [a, *], Hideki Oki [b], Yoshitaka Takagi [a], Tohru Suzuki [a], Akichika Kumatani [a], Ryota Shimizu [a], Masakazu Haruta [a], Takeo Ohsawa [a], Yukio Sato [c], Yuichi Ikuhara [a, c, d], Taro Hitosugi [a, *]

[a] Advanced Institute for Materials Research (AIMR), Tohoku University, 2-1-1 Katahira, Aoba, Sendai, Miyagi 980-8577, Japan
[b] Toyota Corporation, 1200 Mishuku, Susono, Shizuoka 410-1193, Japan
[c] Institute of Engineering Innovation, The University of Tokyo, 2-11-16 Yayoi, Bunkyo, Tokyo 113-8656, Japan
[d] Nanostructures Research Laboratory, Japan Fine Ceramics Center, 2-4-1 Mutsuno, Atsuta, Nagoya 456-8587, Japan

HIGHLIGHTS

- Fabrication of all-solid-state thin film lithium ion secondary battery using epitaxial $LiCoO_2$ thin film.
- Control of crystal orientation of epitaxial $LiCoO_2$ thin film.
- Observation of Li ion insertion/extraction reactions in the thin film battery by cyclic voltammetry measurement.

ARTICLE INFO

Article history:
Received 14 December 2013
Received in revised form
6 May 2014
Accepted 23 May 2014
Available online 6 June 2014

Keywords:
Epitaxial thin films
Lithium-ion batteries
Lithium cobaltite
Crystal orientation
Surface reconstruction

ABSTRACT

We demonstrate the orientation control of $LiCoO_2$ epitaxial thin films deposited on (110)-2 × 1 reconstructed surfaces of Au and Pt by using pulsed laser deposition. The epitaxial $LiCoO_2$ thin films have CoO_2 layers tilted with respect to the surface normal, which is suitable for Li-ion insertion/extraction reactions in $LiCoO_2$. We show the successful operation of all-solid-state thin-film Li-ion batteries by employing the epitaxial $LiCoO_2$ thin films as cathodes. The electrochemical properties of epitaxial films in all-solid-state batteries are improved compared to the batteries using liquid electrolyte.

1. Introduction

Lithium ion batteries (LIBs) have attracted great attention for future electrochemical energy storage devices [1]. Among various types of LIBs, thin film LIBs helps to reduce the physical size of sensors and electric device containing the batteries [2,3]. Hence, many efforts have been devoted toward integration, miniaturization and high performance of thin film batteries. Ideal thin film batteries would be all-solid-state LIBs composed of epitaxial thin films from the viewpoint of high power output, high energy density and safety [4]. Recently, epitaxial thin films of electrode materials such as $LiCoO_2$ (LCO) [5–8], $Li_4Ti_5O_{12}$ [9–11], and $LiMn_2O_4$ [12], have been reported. However, many researchers face difficulties in fabricating all-solid-state epitaxial thin film batteries mainly due to weak adhesion and high interface resistance between the stacked films, and internal short circuit between cathode and anode electrodes. Still now, no report has been done on fabrication and electrochemical evaluation of all-solid-state thin film LIBs composed of epitaxial thin films.

In this study, we report to our knowledge for the first time successful battery operation of all-solid-state thin-film LIB composed of epitaxial cathode thin films. In order to fabricate thin film batteries, it is crucial to control crystal orientation of epitaxial thin films, particularly in the case of electroactive materials with anisotropic transport properties. $LiCoO_2$ (LCO) with a layered-rhombohedral α-$NaFeO_2$ structure has been widely used as a cathode material for commercially available LIBs and is still a promising cathode material for all-solid-state LIBs. In the layered structure of LCO, Li ions show a predominant two-dimensional diffusion along the layers, whereas it is unlikely that Li ions jump

* Corresponding authors.
E-mail addresses: shiraki@wpi-aimr.tohoku.ac.jp (S. Shiraki), hitosugi@wpi-aimr.tohoku.ac.jp (T. Hitosugi).

http://dx.doi.org/10.1016/j.jpowsour.2014.05.133
0378-7753/

to an adjacent Li diffusion layer. Indeed, epitaxial LCO films showed a difference in the charge/discharge capacity, depending on the crystal orientation of LCO [6]. On a $SrTiO_3$(111) substrate, the epitaxial LCO grows with a crystal orientation that the CoO_2 layer is parallel to the substrate, and shows smaller capacity compared to other crystal orientations. Hence, the CoO_2 layer should not be parallel to the substrate surface in fabricating thin film battery using epitaxial LCO. Furthermore, a substrate with metallic conductivity is required to achieve bottom contact in LIBs. However, there has been no report on the control of the LCO crystal orientation on single crystal metal substrates such as Au and Pt.

Here we first demonstrate the epitaxial growth of LCO films deposited on reconstructed (110)-2 × 1 substrate surfaces of Au and Pt by using pulsed laser deposition (PLD). It is well known that the (110) surfaces reconstruct to so-called "missing row" structures with 2 × 1 symmetry [13]. The reconstructed (110) surfaces consist of alternately-arrayed {111} nanofacets (Fig. 1(a)), which lowers the total surface energy since the close-packed {111} facets have the lowest surface energy in case of face-centered cubic materials. By using the missing-row zigzag structures of surface reconstruction, we established a process to control the LCO crystal orientation in such a way that it becomes suitable for smooth Li-ion insertion/extraction reactions. We evaluate electrochemical properties of the orientation-controlled epitaxial LCO thin films using organic liquid electrolyte. Then, we also fabricate all-solid-state thin-film LIBs by depositing thin films of Li phosphorus oxynitride (LiPON) [14] and Li as solid electrolyte and anode on the epitaxial LCO, respectively. We demonstrate the battery operation, and compare the electrochemical properties of the devices by cyclic voltammetry (CV).

2. Experimental

We employed single crystal (110) substrates of Au and Pt, and prepared (2 × 1) reconstructed surfaces by extensive sputtering–annealing cycles in ultrahigh vacuum (UHV) [13]. The surface reconstruction was confirmed by low energy electron diffraction (LEED) and reflection high-energy electron diffraction. The LCO thin films were deposited by using PLD with a polycrystalline $Li_{1.2}CoO_2$ target (Toshima Manufacturing). A KrF excimer laser (wavelength: 248 nm) with a repetition rate of 5 Hz and a fluence of 1.0 J cm^{-2} at the target surface were used for the deposition. During the deposition, the oxygen partial pressure was kept at 1×10^{-6} Torr and the substrate temperature was room temperature (RT). The as-grown samples are epitaxial films, but Li and Co cations are randomly distributed along the c-axis, as discussed by Wang et al. [15] and Bouwman et al. [16]. Hence the as-grown films were subsequently annealed at 650 °C in air to obtain high temperature LCO phase [7]. The LCO films were typically 200 nm thick. The crystal structures of the films were characterized by X-ray diffraction (XRD) (NEW D8 Discover, Bruker), transmission electron microscopy (TEM), and scanning TEM (STEM) (JEM-2010HC and JEM-2100F with an aberration corrector, JEOL Ltd.) [17]. The crystal structures of LCO are indexed on the basis of hexagonal setting, throughout this letter. The electrochemical properties of epitaxial LCO films were examined with coin type Li cells using Li metal foils as anode. The electrolyte used was EC (ethylene carbonate)-DEC (diethyl carbonate) with a molar ratio of 3:7 as a solvent and supporting electrolyte of 1 M $LiPF_6$. The CV measurements were carried out in the voltage range between 3.0 and 4.3 V at a scan rate of 0.1 mV s^{-1}. The cut-off voltages in charge and discharge measurements were 3 and 4.3 V, and the current was set at 1.2 μA (approximately 0.33C). Furthermore, we fabricated all-solid-state thin film batteries using the epitaxial LCO films. A schematic image of the all-solid-state thin film batteries is shown in Fig. 2. The solid electrolyte, LiPON, and anode Li thin films were deposited on the epitaxial LCO films by RF magnetron sputtering (RFMS) and vacuum thermal evaporation (VTE), respectively [3,18,19]. An active area was 5 × 5 mm. After the deposition of LiPON onto LCO, the films were annealed at 180 °C for 30 min in Ar atmosphere to reduce the interface resistance

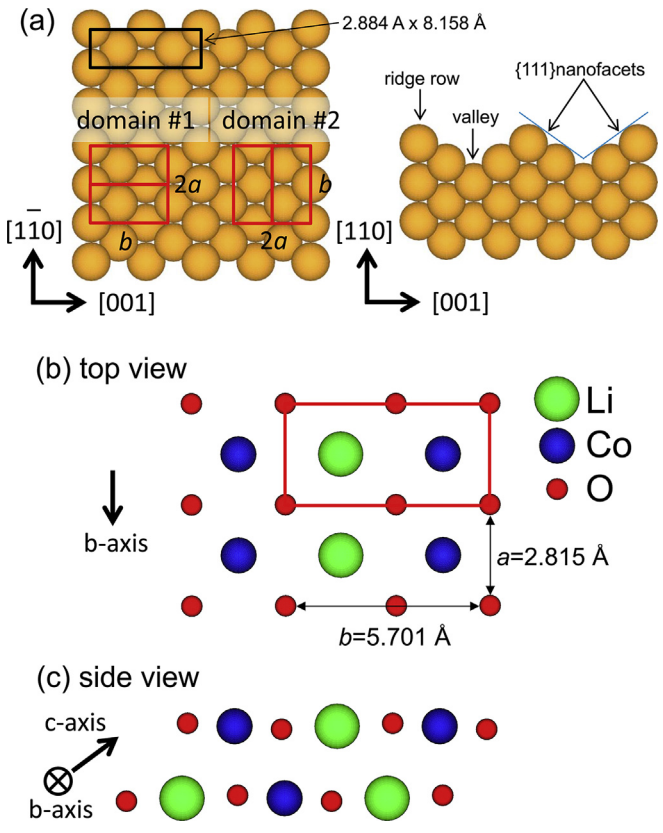

Fig. 1. (a) Schematic view of Au(110)-2 × 1 reconstructed surface and proposed alignment of domains #1 and #2. (b, c) Schematic views of plane of $LiCoO_2$.

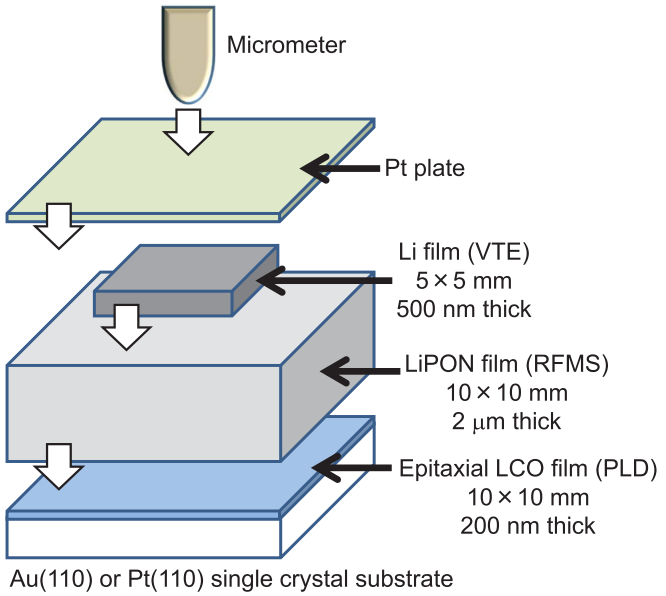

Fig. 2. Schematic image of all-solid-state thin film batteries using epitaxial $LiCoO_2$ thin films on single crystal (110) substrates of Au and Pt.

between LiPON and LCO [18–21]. The preparation of coin cells and electrochemical characterizations of all-solid-state thin film batteries were done in an argon-filled glove box. The electrochemical characterizations were carried out using Solartron 1287 and Bio-Logic SP-150 cell test systems.

3. Results and discussion

We first discuss the growth of LCO on the Au(110)-2 × 1 reconstructed surface. Three different types of orientations (domains #1–3) were found in the epitaxial film. Fig. 3(a) shows an out-of-plane XRD pattern of an LCO thin film. The $(10\bar{1}4)$ peak indicates that the c-axis of LCO is tilted by 54° with respect to the surface normal (Fig. 3(a) inset). It should be noted here that the tilting angle of 54° in LCO is very close to the angle of the {111} nanofacets of Au, i.e., LCO<0003>//Au{111} nanofacets. This result implies that the zigzag structure of {111} nanofacets affects the crystal orientation of LCO. In a θ–2θ scan obtained at $\psi = 54°$ and at ϕ being parallel to [001] direction of Au (Fig. 3(b)), we found (0003), (0006), and (0009) peaks of LCO and deduced the distance of the CoO_2 planes to d = 14.085 Å from the corresponding values of 2θ. The distance d of the film was slightly larger than that of the LCO powder (d = 14.051 Å) [22]. Hereafter we call this domain #1.

Considering a twofold symmetry of reconstructed Au(110) surface (Fig. 1(a), we can expect only two domains of #1-a and #1-b. However, the ϕ-scan of LCO(0003) taken at $\psi = 54°$ (Fig. 3(c)) reveals four peaks: two sharper and two broader reflections. The two sharper peaks of LCO originate from the domains of #1-a and #1-b and the other two reflections arise from the orthogonally oriented domains of #2-a and #2-b. Although both c-axes of domains #1 and #2 are tilted by 54° with respect to the surface normal, the epitaxial relationships are different. As demonstrated later in TEM images, the epitaxial relationship can be described as $[11\bar{2}0]_{LCO}(0001)_{LCO}//[1\bar{1}0]_{Au}(111)_{Au}$ in domains #1-a and #1-b.

Here, we consider the origin of the two broader peaks from domains of #2-a and #2-b. As can be seen in the schematics of the atomic arrangement in the $(10\bar{1}4)$ plane (Fig. 1(b)), the oxygen atoms form nearly a square lattice, thus forming crystallites by an in-plane rotation of 90°. In the case of domains #1 showing sharper peaks, the lattice mismatches between LCO and Au are −2.39% and +4.82% for the $[1\bar{1}0]$ and [001] directions, respectively. On the other hand, the domains #2 showing broader peaks have lattice mismatches of −1.92% and 3.52% for the $[1\bar{1}0]$ and [001] directions, respectively. In spite of the larger mismatches, the crystallinity of domains #1 is better than that of domains #2. This fact also implies that the missing-row zigzag structure of the reconstructed surface assists the stable formation of domains #1.

The evidence of the third phase (domain #3) can be found in a θ–2θ scan taken at $\psi = 37°$ (Fig. 4(a)). We clearly see a (0003) peak of LCO in addition to a (111) peak from the Au substrate. This indicates the growth of small LCO domains #3 with another type of crystal orientation that the c-axis of LCO is perpendicular to the {111} nanofacets of the reconstructed surface. Fig. 4(b) shows ϕ-scans of LCO(0003) and Au(111) taken at $\psi = 37°$. Two peaks of LCO(0003) are observed along the <111> directions of Au, supporting the epitaxial growth of LCO(0003) on the {111} nanofacets. This result is understandable considering the fact that (0001)-oriented thin films grow on Au(111)/Si substrates [23]. Taken together, we found three types of epitaxial crystallites and six types of domains in the LCO film. No impurity phase, such as CoO, Co_2O_3, Co_3O_4, or $LiCo_2O_4$, was observed. In the domains #1 and #2, the c-axes are tilted by 54° with respect to the surface normal, and particularly the domains #1 grow with its c-axis parallel to the

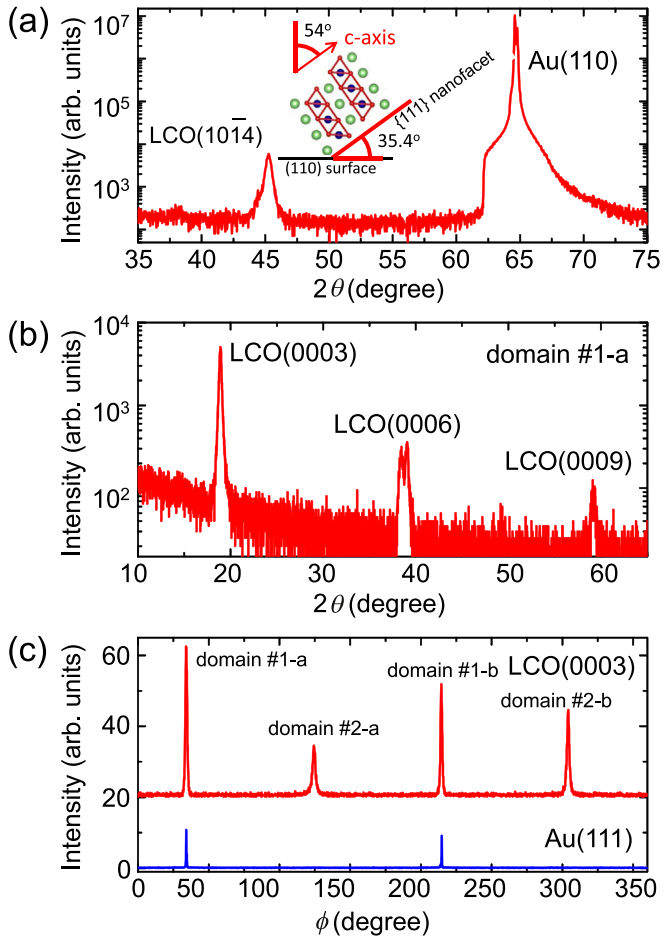

Fig. 3. (a) Out-of-plane XRD patterns of $LiCoO_2$ thin film on a Au(110)-2 × 1 reconstructed surface. The inset shows the crystal alignment of CoO_2 layers (domain #1) and substrate. (b) θ–2θ scan obtained at $\psi = 54°$. (c) ϕ-scan of $LiCoO_2$(0003) and Au(111) planes obtained at $\psi = 54°$ and 37°, respectively.

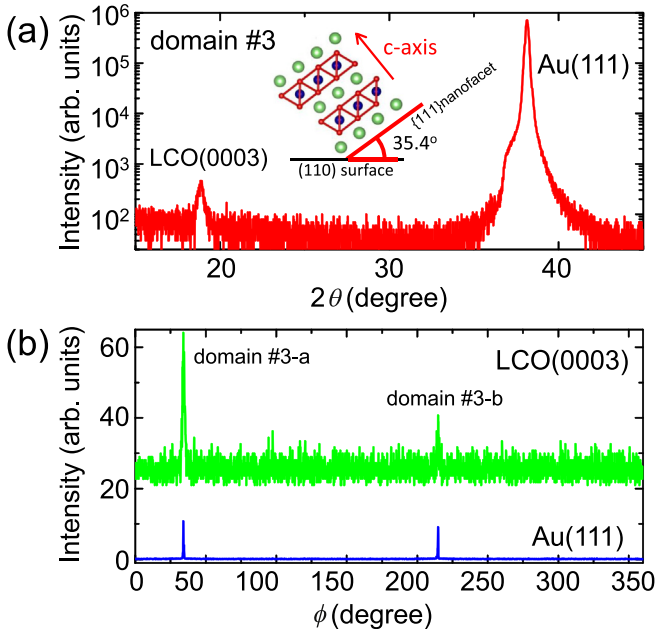

Fig. 4. (a) θ–2θ scan obtained at $\psi = 37°$. (b) ϕ-scan of $LiCoO_2$(0003) and Au(111) planes obtained at $\psi = 37°$.

{111} nanofacets of Au(110). In contrast, the domains #3 epitaxially grow with its c-axis perpendicular to the {111} nanofacets, and its volume fraction is estimated to be approximately 14%. As shown in the insets of Figs. 3(a) and 4(a), the CoO_2 planes of the domains #1 and #3 are perpendicular and parallel to the {111} nanofacets of Au, respectively.

Fig. 5(a) shows an out-of-plane XRD pattern of an LCO thin film deposited on the Pt(110)-2 × 1 reconstructed surface. The XRD results of LCO thin films on Au(110)-2 × 1 and Pt(110)-2 × 1 reconstructed surfaces indicated very similar properties. In Fig. 5(a), the $(10\bar{1}4)$ peak clearly appears, and the c-axis of LCO is tilted by 52° with respect to the surface normal (Fig. 5(a) inset). The distance d and tilting angle of c-axis are slightly different from the case on Au(110). From a θ–2θ scan obtained at $\psi = 52°$ and at ϕ being parallel to [001] direction of Pt (Fig. 5(b)), we deduced the distance of the CoO_2 planes to $d = 14.117$ Å, which is larger than that found on Au although the lattice constant of Pt is smaller than Au (Table 1). Concerning the domains #3, the same tendency was observed for LCO on Pt(110), as shown in Fig. 6.

A more elaborate structural analysis was made using TEM and STEM. Fig. 7(a) shows a bright-field TEM image of LCO/Au(110) taken along the $[1\bar{1}0]$ zone axis of Au. The surface of the LCO film is almost flat, and the surface roughness Ra was estimated to be 3.6 nm from atomic force microscopy (AFM) measurements. A selected area electron diffraction (SAED) pattern in Fig. 7(b) is characterized by the overlap of sharp lattices from Au and LCO. Out of the three domains in LCO, domains #1 and #3 can have the $[11\bar{2}0]$ axis oriented parallel to the [110] direction of Au, while domains #2 do not show this type of alignment. Therefore, if the interface is oriented along the Z = [110] zone axis of Au, the Z = zone axis pattern of LCO can be simultaneously obtained only for the domains #1 and #3. However, only the pattern from domains #1 was observed, indicating that the domains #1 are dominant in this region. Considering the size of electron beam in TEM experiments, the size of domains #1 is about 2 μm in width. A high-resolution STEM image of the LCO/Au interface in Fig. 7(c) reveals that the interface is nearly flat, and no impurity phase appears such as Co_3O_4 at the interface. It is clear that the CoO_2 planes are tilted with respect to the {111} plane of Au, and this region belongs to domain #1, consistent with the SAED result.

Table 1
Distance d of epitaxial $LiCoO_2$ films.

	Domain #1 and #2 [Å]	Domain #3 [Å]
Au(110) (a = 4.079 Å)	14.085	14.103
Pt(110) (a = 3.924 Å)	14.117	14.166

The TEM and STEM results obtained for LCO/Pt(110)-2 × 1 show more clear images. As shown in Fig. 8(a), the surface of the LCO film is almost flat, but is partially composed of facets, as indicated by an arrow. The surface roughness Ra was estimated to be 1.7 nm from AFM measurements. The LCO film shows domain boundaries vertical to the substrate plane and pillar-shaped domains with a few tens of nm in width. The SAED pattern in Fig. 8(b) is characterized by the overlap of a sharp triangular lattice from Pt and circular arcs from LCO. Similarly to the LCO on Au(110), the Z = zone axis pattern of LCO can be simultaneously obtained only for the domains #1 and #3. Basically, the c-axes of the domains #1 and #3 are rotated by 52° and 37° with respect to the surface normal, respectively. However, the rotation angle is not strongly fixed to these values and variation is allowed. A sequential variation of the c-axis rotation angle results in circular arcs instead of sharp distinct spots in the

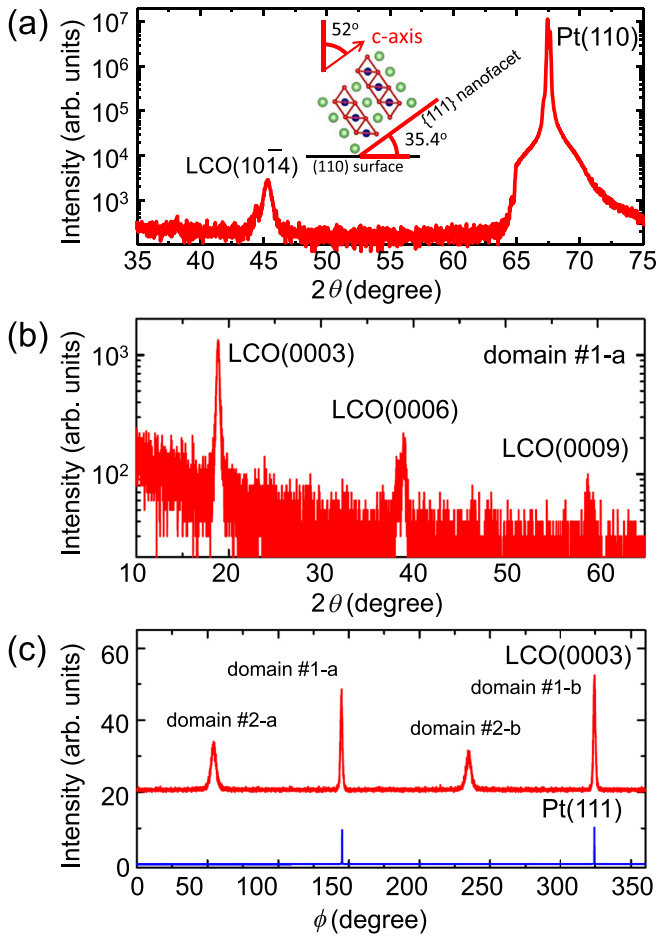

Fig. 5. (a) Out-of-plane XRD patterns of $LiCoO_2$ thin film on a Pt(110)-2 × 1 reconstructed surface. The inset shows the crystal alignment of CoO_2 layers (domain #1) and substrate. (b) θ–2θ scan obtained at $\psi = 52°$. (c) ϕ-scan of $LiCoO_2$(0003) and Pt(111) planes obtained at $\psi = 52°$ and 37°, respectively.

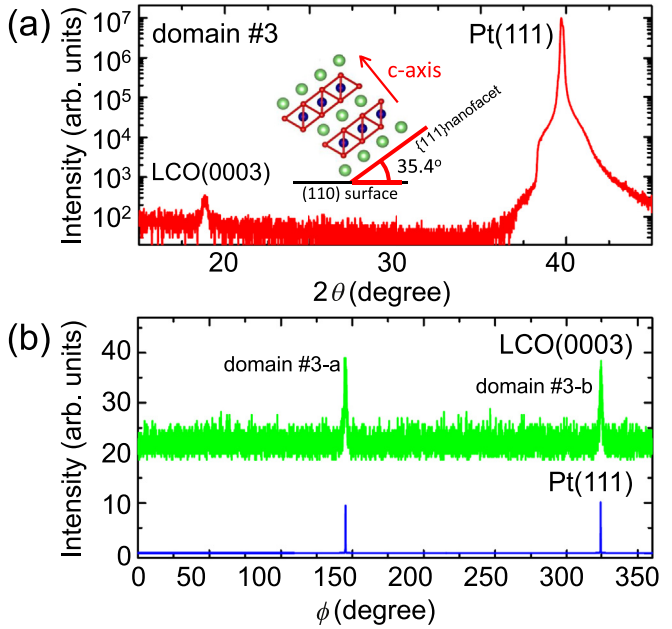

Fig. 6. (a) θ–2θ scan obtained at $\psi = 37°$. (b) ϕ-scan of $LiCoO_2$(0003) and Pt(111) planes obtained at $\psi = 37°$.

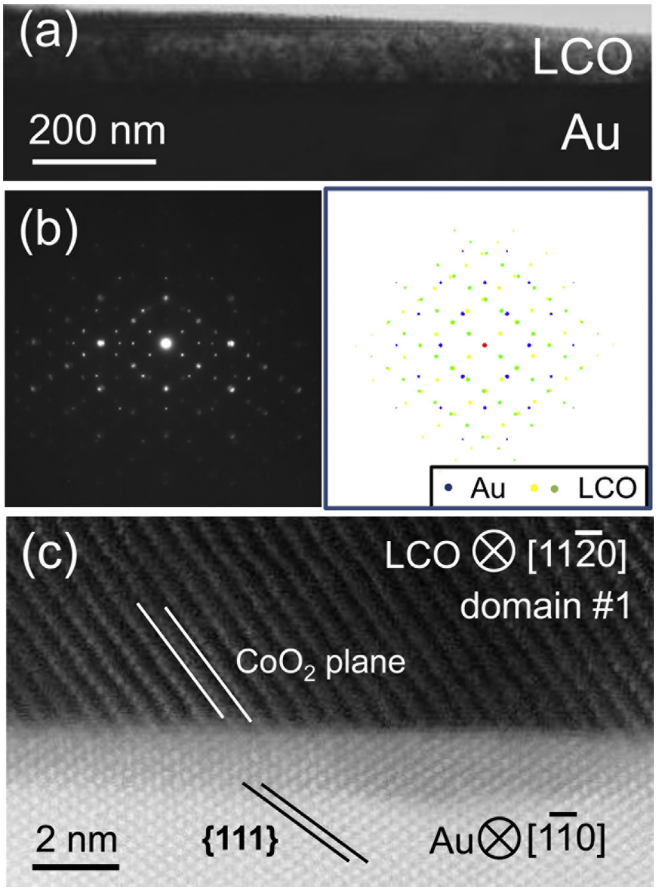

Fig. 7. (a) Bright-field TEM image of $LiCoO_2$/Au(110). (b) Selected area electron diffraction pattern from $LiCoO_2$ film. Left panel: experimental pattern. Right panel: schematic of the respective components. (c) High-resolution STEM image of $LiCoO_2$ (domain #1)/Au interface. All the TEM images and diffraction pattern were taken along [1$\bar{1}$0] zone axis of Au.

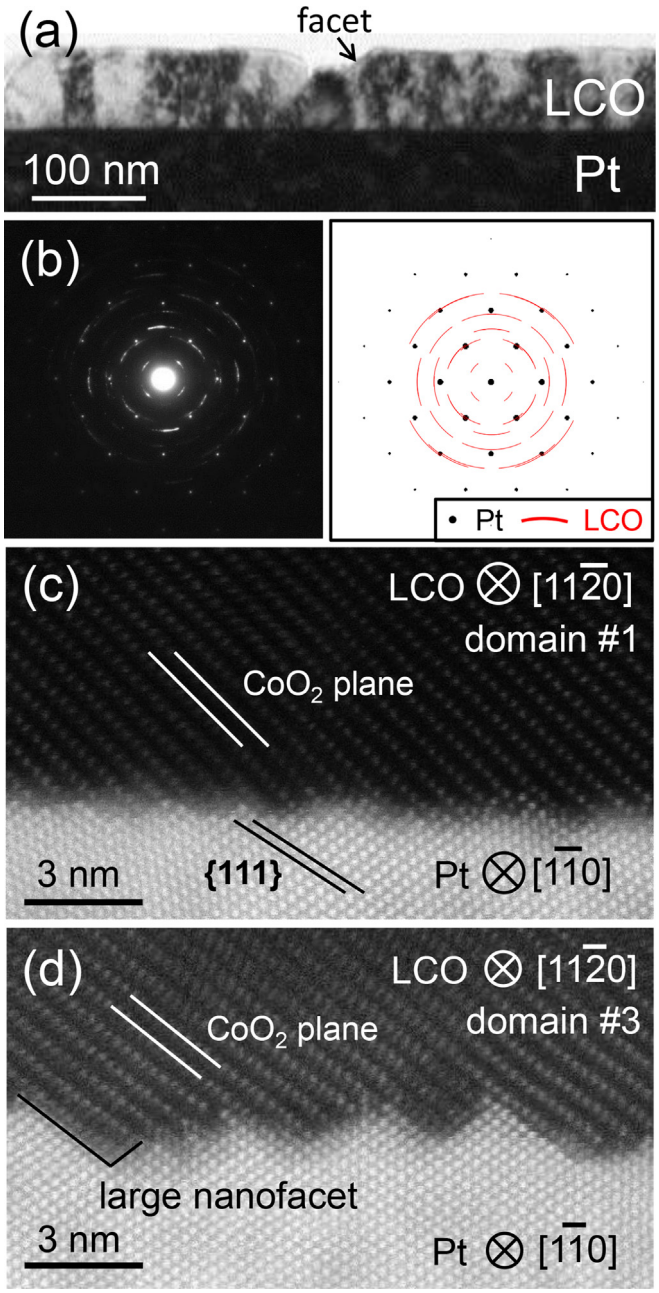

Fig. 8. (a) Bright-field TEM image of $LiCoO_2$/Pt(110). (b) Selected area electron diffraction pattern from $LiCoO_2$ film. Left panel: experimental pattern. Right panel: schematic of the respective components. (c) High-resolution STEM image of $LiCoO_2$ (domain #1)/Pt interface. (d) High-resolution STEM image of $LiCoO_2$ (domain #3)/Pt interface. All the TEM images and diffraction pattern were taken along [1$\bar{1}$0] zone axis of Pt.

SAED pattern. An inspection of the SAED results reveals that the c-axis rotation angle ranges from approximately 35°–65° with respect to the surface normal, which approximately agrees with the XRD results. In addition, the LCO film has a double-domain structure (#1(3)-a and #1(3)-b) owing to the twofold symmetry of the (110)-2 × 1 surface. Therefore, two types of circular arcs exist in the pattern. The STEM image of the LCO/Pt interface in Fig. 8(c) shows that the interface is nearly atomically flat but has some fine zigzag features owing to the (110)-2 × 1 reconstructed surface of Pt that was evidenced by LEED. No impurity phase such as Co_3O_4 appears at the interfaces. Clearly, the CoO_2 planes are tilted with respect to the {111} plane of Pt, and this region belongs to domain #1. On the other hand, the STEM image in Fig. 8(d) reveals the CoO_2 planes of LCO are parallel to the {111} plane of Pt and indicates that this region belongs to domain #3. In this region, the 2 × 1 reconstruction is not perfect and the large {111} nanofacets are formed. It seems that the domains #3 dominantly grow on the large {111} nanofacet region. This tendency implies fine surface structure of substrates plays an important role in growth manner and crystal orientation of epitaxial films.

We examined electrochemical properties of the orientation-controlled LCO epitaxial films. Fig. 9(a) shows CV curves of the Li cells with LCO films and liquid electrolyte. The six peaks at 3.96 (C1), 4.08 (C2), 4.20 (C3), 3.86 (D1), 4.04 (D2), and 4.16 V (D3) during charge/discharge cycles correspond to the insertion/extraction of Li ions in LCO [24–27]. The C1 and D1 peaks are two-phase reactions, whereas the others are single-phase reactions. The CV curves drastically change in shape with cycle. Subsequently, we measured the charge and discharge curves of Fig. 9(b) showing good reversibility between 3 and 4.3 V.

We further fabricated all-solid-state battery by depositing a thin film of LiPON as a solid electrolyte (2 μm thick) and a thin Li film as an anode (500 nm) on top of the LCO/Au(110)-2 × 1 device with an active area of 5 × 5 mm. Iriyama et al. reported that film batteries exhibited stable CV curves compared to conventional systems using liquid electrolyte [19]. Hence, the CV measurements were carried out in the voltage range 3.0–4.3 V at a scan rate of 0.1 mV s^{-1}. The CV curves in Fig. 10(a) show several sharp peaks (C1-4, D1-3), and

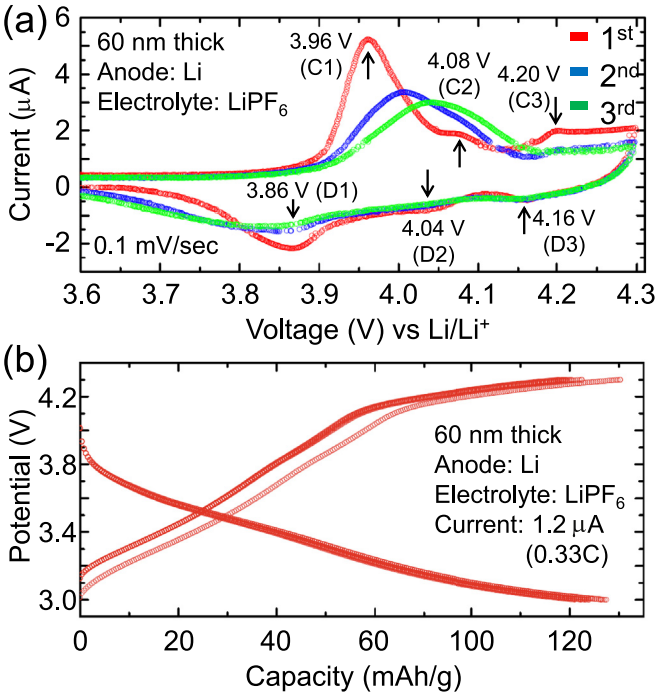

Fig. 9. Electrochemical properties of epitaxial $LiCoO_2$ thin film on Au(110) with liquid electrolyte $LiPF_6$. (a) Cyclic voltammogram at a scan rate of 0.1 mV s^{-1}. (b) Charge and discharge curves at the current of 1.2 μA (0.33C). 6 cycles are plotted.

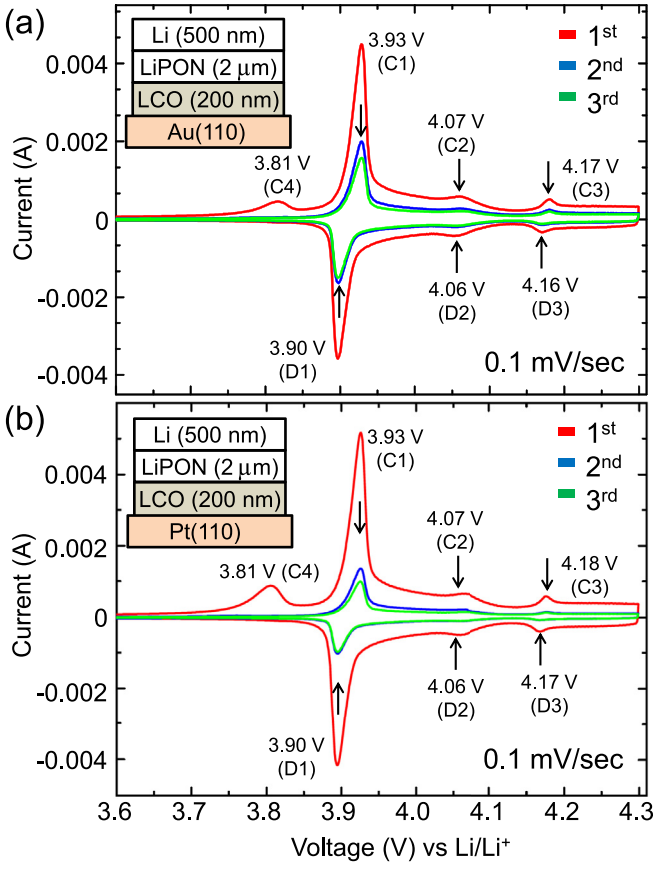

Fig. 10. Cyclic voltammogram of thin-film solid-state battery of Li/LiPON/epitaxial $LiCoO_2$ on Au(110) (a) and on Pt(110) (b). The insets show stacking of thin films.

Table 2
Peak voltages and peak separation in CVs [V].

	C1	C2	C3	D1	D2	D3	C1-D1	C2-D2	C3-D3
LCO with $LiPF_6$ on Au(110)	3.96	4.08	4.20	3.86	4.04	4.16	0.10	0.04	0.04
LCO with LiPON on Au(110)	3.93	4.07	4.17	3.90	4.06	4.16	0.03	0.01	0.01
LCO with LiPON on Pt(110)	3.93	4.07	4.18	3.90	4.06	4.17	0.03	0.01	0.01

are similar to the result of Fig. 9(a). We also see an additional peak (C4) at the lowest voltage of 3.81 V. This peak appears only during the first positive scan, and therefore, does not seem to be directly related to the reaction of Li in LCO. Although the current is reduced at the second scan, as compared to the first one, the second and third cycles are almost the same. Furthermore, the fact that all the charge and discharge peak voltages do not change also indicates good stability and repeatability in battery operation, in contrast to the CV curves in Fig. 9(a). In particular, the peak separations (C1-D1, C2-D2, C3-D3) between charge and discharge reactions are smaller than those obtained using liquid electrolyte (Table 2). In Fig. 10(b), the CV curves of Li/LiPON/LCO/Pt(110) are shown for comparison. Although the distance *d* of the LCO films are slightly different, the CV curves show the same tendency. The peak voltages and peak separations are almost same as the values found for Li/LiPON/LCO/Au(110). Finally, we consider the effects of orientation-controlled epitaxial thin films on electrochemical properties. Iriyama et al. and Kuwata et al. already reported the electrochemical properties of all-solid-state thin film batteries using the (0003)-oriented polycrystalline LCO thin films [18,19,26,27]. Compared with the polycrystalline LCO thin films, the CV curves of Fig. 10 seem to show sharper reaction peaks. Furthermore, the peak separations of 0.01 V for two-phase reactions (Table 2) are much smaller than the values found for the polycrystalline samples. This result indicates that the reactivity is improved probably due to the tilted crystal orientations in the epitaxial LCO thin films.

To sum up, the impact of the successful battery operation achieved in this research can pave the way to investigate epitaxial electrode/electrolyte interfaces. One of the most serious drawbacks that hinder the practical use of all-solid-state LIBs is the low Li-ion conductance at the electrode/electrolyte interface. Recent investigations show an improved conductance at the interfaces by coating the electrodes with other materials [28–30]. However, the mechanisms leading to an enhanced conductance and the material design principle of the interface are not well understood. The epitaxial thin films offer ideal well-defined interfaces for studying such mechanisms as well as the effects of crystal orientation and domain boundaries in active materials and electrolytes on electrochemical properties [31]. These studies would give further insight into the Li-ion conduction mechanism in batteries, which is the key issue for the application of all-solid-state LIBs.

4. Conclusion

We successfully controlled the crystal orientation of $LiCoO_2$ on the (110)-2 × 1 reconstructed substrate surfaces of Au and Pt to obtain the most appropriate orientation for ion conduction in LCO. The XRD and TEM results clearly indicate the epitaxial growth of LCO thin films with three different types of crystal orientations, in which the c-axes of LCO are tilted with respect to the surface normal. The electrochemical properties of orientation-controlled epitaxial films were examined using organic liquid electrolyte. Furthermore, we fabricated all-solid-state thin film LIBs using the epitaxial LCO thin films, and confirmed the stable battery operation

of the devices. The electrochemical properties of epitaxial films in all-solid-state batteries showed sharp reaction peaks and small peak separations, which is much improved compared to the case using liquid electrolyte. These studies pave the way to a detailed understanding of solid electrode/electrolyte interfaces, which is a critical factor in determining the Li-ion mobility in all-solid-state LIBs.

Acknowledgments

This study was supported by the Japan Society for the Promotion of Science (JSPS) through its Funding Program for World-Leading Innovation R&D on Science and Technology (FIRST Program). S. S. acknowledges a Grant-in-Aid for Scientific Research (No. 25390072) from the Ministry of Education, Culture, Sports, Science and Technology (MEXT), Japan.

References

[1] Basic Research Needs for Electrical Energy Storage, Department of Energy, The United States of America, 2007.
[2] K. Kanehori, K. Matsumoto, K. Miyauchi, T. Kudo, Solid State Ionics 9–10 (1983) 1445–1448.
[3] B. Wang, J.B. Bates, F.X. Hart, B.C. Sales, R.A. Zuhr, D. Robertson, J. Electrochem. Soc. 143 (1996) 3203–3213.
[4] K. Takada, Acta Mater. 61 (2013) 759–770.
[5] K. Nishio, T. Ohnishi, K. Akatsuka, K. Takada, J. Power Sources 247 (2014) 687–691.
[6] M. Hirayama, N. Sonoyama, T. Abe, M. Minoura, M. Ito, D. Mori, A. Yamada, R. Kanno, T. Terashima, M. Takano, K. Tamura, J. Mizuki, J. Power Sources 168 (2007) 493–500.
[7] T. Tsuruhama, T. Hitosugi, H. Oki, Y. Hirose, T. Hasegawa, Appl. Phys. Express 5 (2009) 085502.
[8] T. Ohnishi, B.T. Hang, X. Xu, M. Osada, K. Takada, J. Mater. Res. 25 (2010) 1886–1889.
[9] M. Hirayama, K. Kim, T. Toujigamori, W. Cho, R. Kanno, Dalt. Trans. 40 (2011) 2882–2887.
[10] A. Kumatani, T. Ohsawa, R. Shimizu, Y. Takagi, S. Shiraki, T. Hitosugi, Appl. Phys. Lett. 101 (2012) 123103.
[11] A. Kumatani, S. Shiraki, Y. Takagi, T. Suzuki, T. Ohsawa, X. Gao, Y. Ikuhara, T. Hitosugi, Jpn. J. Appl. Phys. 53 (2014) 058001.
[12] N. Sonoyama, K. Iwase, H. Takatsuka, T. Matsumura, N. Imanishi, Y. Takeda, R. Kanno, J. Power Sources 189 (2009) 561–565.
[13] W. Moritz, D. Wolf, Surf. Sci. 88 (1979) L29–L34.
[14] J.B. Bates, N.J. Dudney, G.R. Gruzalski, R.A. Zuhr, A. Choudhury, C.F. Luck, Solid State Ionics 53-56 (1992) 647–654.
[15] H. Wang, Y.-I. Jang, B. Huang, D.R. Sadoway, Y.-M. Chiang, J. Electrochem. Soc. 146 (1999) 473–480.
[16] J. Bouwman, B.A. Boukamp, H.J.M. Bouwmeester, H.J. Wondergem, P.H.L. Notten, J. Electrochem. Soc. 148 (2001) A311–A317.
[17] R. Huang, T. Hitosugi, S.D. Findlay, C.A.J. Fisher, Y.H. Ikuhara, H. Moriwake, H. Oki, Y. Ikuhara, Appl. Phys. Lett. 98 (2011) 051913.
[18] Y. Iriyama, T. Kako, C. Yada, T. Abe, Z. Ogumi, Solid State Ionics 176 (2005) 2371–2376.
[19] Y. Iriyama, T. Kako, C. Yada, T. Abe, Z. Ogumi, J. Power Sources 146 (2005) 745–748.
[20] J.B. Bates, N.J. Dudney, B.J. Neudecker, F.X. Hart, H.P. Jun, S.A. Hackney, J. Electrochem. Soc. 147 (2000) 59–70.
[21] B.J. Neudecker, N.J. Dudney, J.B. Bates, J. Electrochem. Soc. 147 (2000) 517–523.
[22] H. Wang, Y.-I. Jang, B. Huang, D.R. Sadoway, Y.-M. Chiang, J. Power Sources 81 (1999) 594–598.
[23] Y.J. Kim, E.-K. Lee, H. Kim, J. Cho, Y.W. Cho, B. Park, S.M. Oh, J.K. Yoon, J. Electrochem. Soc. 151 (2004) A1063–A1067.
[24] I. Uchida, H. Sato, J. Electrochem. Soc. 142 (1995) L139–L141.
[25] K.W. Kim, S.I. Woo, K.-H. Choi, K.-S. Han, Y.-J. Park, Solid State Ionics 159 (2003) 25–34.
[26] N. Kuwata, N. Iwagami, Y. Tanji, Y. Matsuda, J. Kawamura, J. Electrochem. Soc. 157 (2010) A521–A527.
[27] N. Kuwata, N. Iwagami, Y. Matsuda, Y. Tanji, J. Kawamura, ECS Trans. 16 (2009) 53–60.
[28] N. Ohta, K. Takada, L. Zhang, R. Ma, M. Osada, T. Sasaki, Adv. Mater. 18 (2006) 2226–2229.
[29] Y. Iriyama, H. Kurita, I. Yamada, T. Abe, Z. Ogumi, J. Power Sources 137 (2004) 111–116.
[30] D. Takamatsu, S. Mori, Y. Orikasa, T. Nakatsutsumi, Y. Koyama, H. Tanida, H. Arai, Y. Uchimoto, Z. Ogumi, J. Electrochem. Soc. 160 (2013) A3054–A3060.
[31] E.Y. Tsymbal, E.R.A. Dagotto, C.B. Eom, R. Ramesh, Multifunctional Oxide Heterostructures, Oxford University Press, 2012.